Seismic Behavior of Plate Reinforced Connections

A. Deylami, M. Tehranizadeh, M. Gholami & H. Moazemi
Amirkabir University of Technology, Iran

SUMMARY:
This study elucidates the behavior of flange plate connection between a steel beam and a welded box column. Four finite element models simulating an exterior connection were prepared and analyzed. On the base of finite element results, two flange plate connection details which are the reinforcing plate length and plate-to-flange fillet weld geometry were improved. Then, two full-scale specimens with flange plate connections were tested using a standard connection requalification test protocol. The flange plate connections of test specimens achieved the AISC seismic provision requirements for special moment frames.

keywords: Connections; Flange Plate; Box Columns; Experimental program; Finite element.

1. INTRODUCTION

Box columns are frequently employed in areas of high seismic risk because they have an excellent capacity to resist biaxial bending. Cold-formed hollow sections are often used for low and medium rise buildings and built-up sections made up of four plates welded together are used for high rise buildings (Nakashima et al, 2000). Extensive studies have been carried out and several new connection details have been proposed for the connection of I-beams to wide flange columns since the 1994 Northridge earthquake (Kim et al, 2002, Ricles et al, 2002, Chen et al, 2005, Tabar et al, 2004, Shiravand et al, 2010, Adeli et al, 2011). But limited research for the connection of I-beams to box–columns has been conducted (Chen et al, 2004). Kim et al. (2004) tested two full-scale moment connections to US box columns fabricated using pre-Northridge connection details. Test results revealed that both specimens failed by brittle fracture of complete joint penetration (CJP) welds between the beam flange and the column during a story drift angle of less than 1% rad, which resulted in no plastic rotation in the connections. Chen et al (2004) tested six large scale specimens of steel beam-to-box column connections. One of the test specimens was the unreinforced connection using pre-Northridge details, and other test specimens were the reinforced connections using rib plates or wing plates. The unreinforced connection was failed by fracture in the heat affected zone (HAZ) of the beam bottom flange during 2.3% story drift angel cycle.

In the present study the behavior of welded flange plate (WFP) connection, shown in Fig. 1, has been investigated.. The geometry of these plates is considered in a manner that site welding in a horizontal position is possible for connecting flange plates to beam and column. This study analytically and experimentally investigates the behavior of the WFP connections. On the base of finite element results, an improved WFP connection was proposed. Then, two full-scale specimens with flange plate connections were tested using a standard connection prequalification test protocol. The results of the specimen's hysteretic behavior were obtained and compared to the AISC seismic provision requirements in order to qualify the improved flange plate connection.

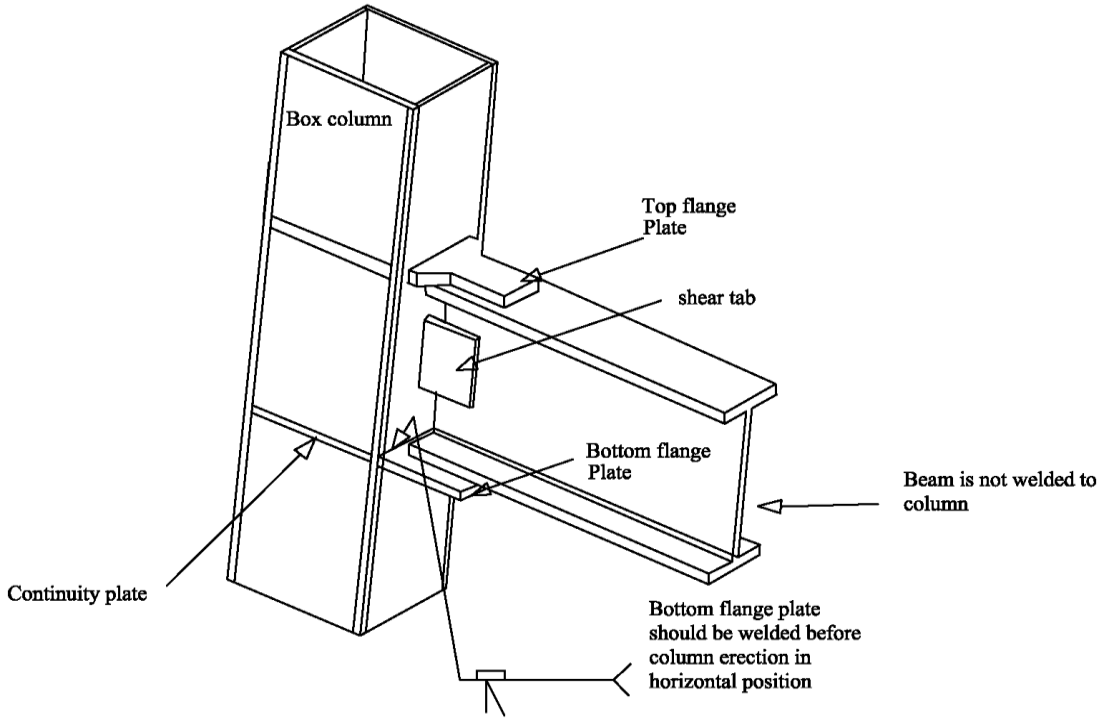

Figure 1. Field welded moment connection.

2. NONLINEAR FINITE-ELEMENT ANALYSIS

Finite-element analysis can provide considerable insight into behavior of complex connections even though the analysis cannot readily address material imperfections, geometric imperfections, residual stresses and strains, and defects.

2.1. Finite element models

Four models were prepared to simulate an exterior T-shaped joint subassembly. The general configuration of the exterior joint subassembly is shown in Fig. 2. All models consisted of a H-shaped steel beam with the dimensions of H-380×200×8×12 (mm) connected to a box column with the measurements of B-400 × 400 × 20 × 20 (mm). The width-thickness ratios of the beam flange and the web are 8.33 and 44.5, respectively, and the beam section categorizes to a compact section, which is capable of developing the fully plastic stress distribution. Summary information on models is presented in Table 2.1. Model UN represents an unreinforced connection. In the remaining three models, the joint from the steel beam to the box column was a WFP moment connection. Fig. 3 shows connection details of model LF30. In the model LF30, flange plates were joined to the beam flanges with longitudinal fillet welds only. Model LF30-T was identical to LF30 except for the addition of the transverse fillet weld at the nose of the flange plate; the size of the LF30-T fillet welds was smaller than that of LF30 to preserve the total volume of fillet weld material. Fig. 4 is a plan view of the fillet welds of LF30 and LF30-T. Model LF50-T was most similar to model LF30-T except that the flange-plate length was arbitrarily increased from 300 to 500 mm.

As shown in Fig. 5, groove welds and fillet welds were modeled. The beam, column, plates, CJP groove welds and fillet welds in the model were discretized using three-dimensional solid (brick) elements. The size of the finite-element mesh varied over the length and height of the specimen. A fine- mesh was used near the connection of the beam to the column and the beam flange to the reinforcing plate. A coarser mesh was used elsewhere. Most of the solid elements were right-angle

prisms. Hinged boundary conditions were used to support the column top and bottom. The load was applied by imposing incremental vertical displacements at the beam tip during the analysis.

A bilinear stress–strain relationship was considered for each of materials. Table 2.2 presents the material properties used for the analytical models. Data from test of coupon extracted from the beam of test specimen LF30-T were used to establish the stress-strain relationship for the steel material. The weld material was modeled using the test data of Kaufmann (1997). The Poisson's ratio was taken as 0.3 for all materials throughout the analyses. To account for material nonlinearities, the von mises yield criterion was employed.

2.2. Rupture index

To compare between the behavior of the different configurations analyzed in this research, a rupture index was used and computed for different cases; this same methodology and approach was used by others (Kim et al, 2002, Ricles et al, 2003, Mao et al, 2002). The rupture index (RI) is defined as:

$$\mathrm{RI} = \frac{\mathrm{PEEQ}}{\exp(-1.5\frac{\sigma_m}{\bar{\sigma}})} \qquad (2.1)$$

Where PEEQ, σ_m and $\bar{\sigma}$ are, respectively, the equivalent plastic strain, hydrostatic stress, and von mises stress. The rupture index was introduced by Hancock and Mackenzie (1976). Locations in a connection with higher values of RI have a greater potential for ductile fracture

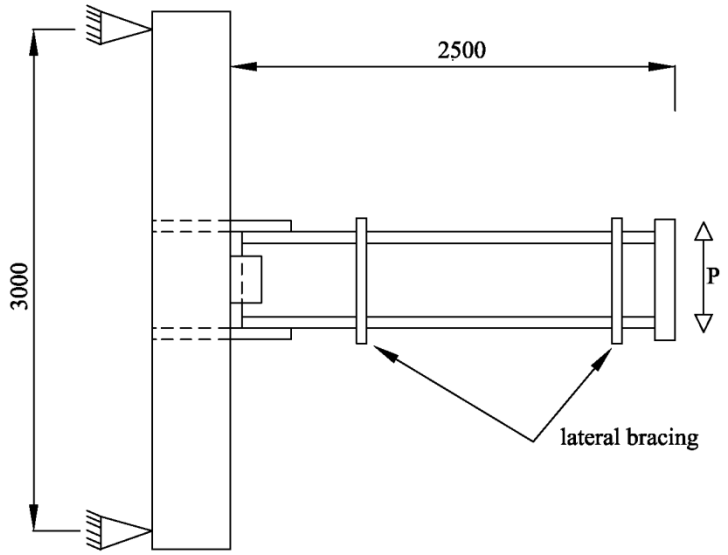

Figure 2. Configuration of the exterior joint subassembly

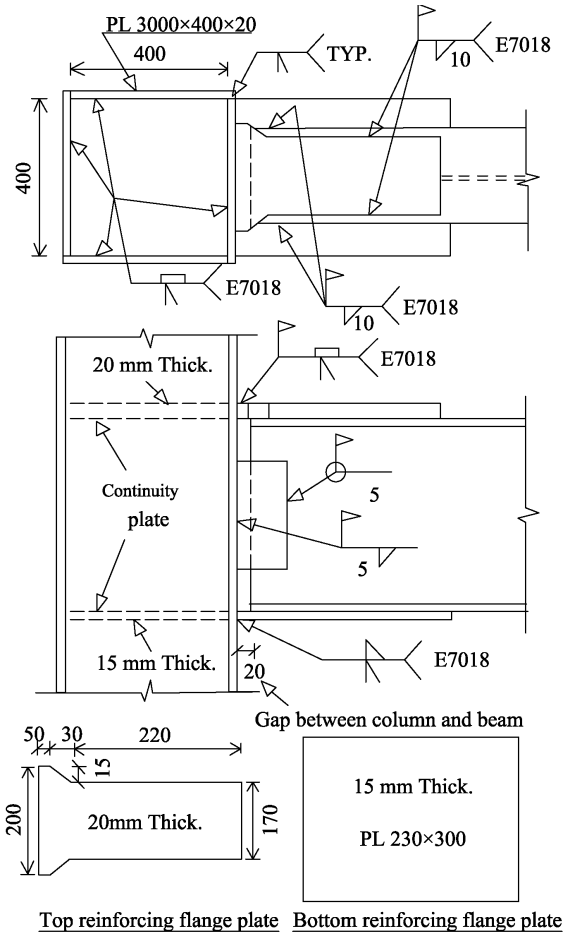

Figure 3. Connection details of model LF30

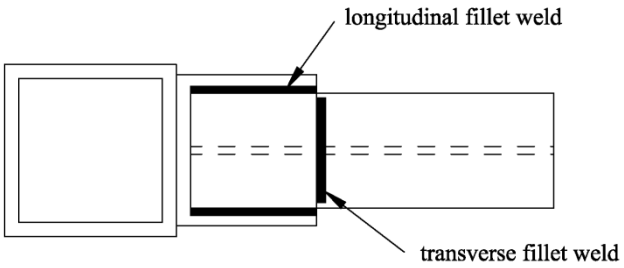

a)

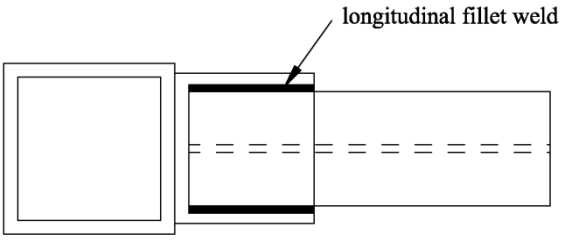

b)

Figure 4. Fillet weld geometry: (a) LF30-T and (b) LF30

Table 2.1. Summary Information on Models

Model	Connection type	flange-plate length	Top flange-plate thickness	Bottom flange-plate thickness	longitudinal fillet weld	transverse fillet weld
UN	Unreinforced	-------	-------	-------	-------	-------
LF30	Flange plate	300	20	15	10	-------
LF30-T	Flange plate	300	20	15	8	8
LF50-T	Flange plate	500	25	20	8	8

Note: All dimensions in mm.

2.3. Analytical results

A story drift angle of 4% rad was used to compare the connection behaviors under highly strained states because a special moment-resisting frame is assumed to be capable of sustaining a story drift angle of at least 4% rad.

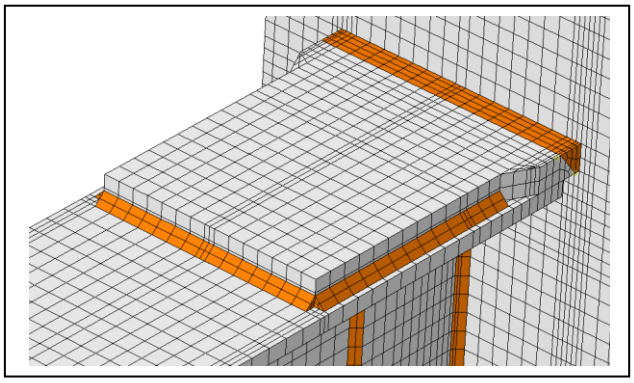

Figure 5. Finite element model

Table 2.2. Material properties

	Yield point		Ultimate point	
Material	σ_y	ε_y	σ_u	ε_u
Steel	3000	0.15	4200	18
Weld	5200	0.26	5600	12

2.3.1. Comparison between the behavior of unreinforced and flange plate connections

To compare between the behavior of unreinforced and reinforced connections, the finite element models of LF30-T and UN were studied.
Fig. 6 presents information on the distributions of the RI for models UN and LF30-T at the face of the column. The maximum value of the RI of UN is approximately 0.22 and is recorded at the edge of the beam flange. The largest value of RI is approximately 0.05 for LF30-T. The maximum value of the RI of UN is approximately four times greater than that of LF30-T. This indicates that the use of the flange plate connection will reduce the likelihood of ductile fracture of steel moment-resisting connections as compared to the unreinforced connection.

2.3.2. Influence of connection details on the response of connection

2.3.2.1. Fillet weld geometry

Two fillet weld (two-sided and three-sided) profiles were studied in this research. To compare the fillet weld profiles, the responses of two specimens LF30 (L-L fillet weld), LF30-T (L-L-T fillet weld), are compared below.
Fig. 7 shows the distributions of the RI for LF30 and LF30-T on the beam bottom flange at the nose of the bottom reinforcing plate. As can be seen in the Fig. 7, the maximum value of the RI is recorded at

the end of the longitudinal fillet weld of LF30. The maximum value of the RI is 0.45 for LF30, whereas its value is merely 0.2 for LF30-T. This reveals that addition of the transverse fillet weld at the nose of the flange plate substantially reduces the maximum value of the RI. There is a possible explanation for this phenomenon:

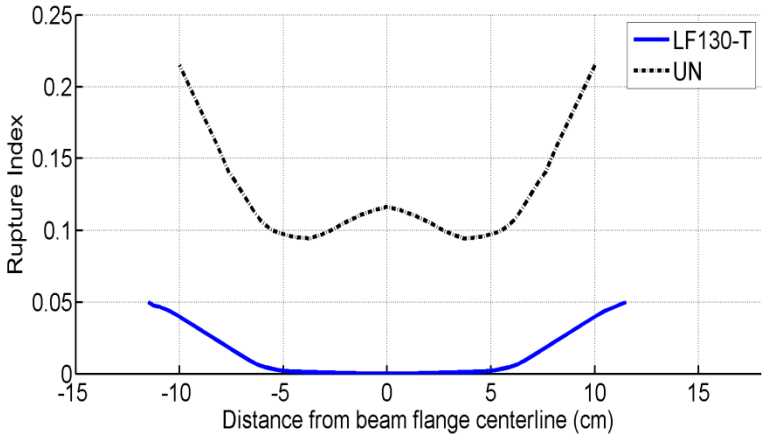

Figure 6. Distribution of rupture index at the face of the column for models UN and model LF30-T

Consider the 2-sided fillet weld (longitudinal fillet welds only) and the end of the fillet weld at the nose of the reinforcing plate. The gap between the beam flange and the reinforcing plate at the bottom of the vertical leg of the fillet weld acts as an initial defect. The resulting stress concentrations and a state of triaxial tension at the end of the longitudinal fillet weld substantially increase the RI values. The addition of a transverse fillet weld eliminates the defect at the base of the vertical leg of the longitudinal fillet weld and reduces the stresses and triaxial tension at the end of the longitudinal fillet weld.

Construction-related issues aside and based on the ABAQUS analysis data only, the 3-sided fillet weld (2 longitudinal welds and 1 transverse weld) is superior to the 2-sided fillet weld (2 longitudinal welds).

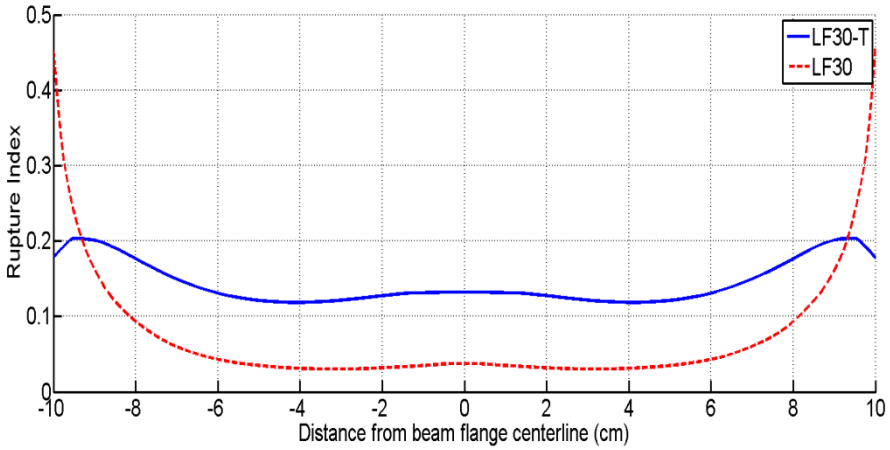

Figure 7. Distribution of rupture indices on beam flange at the nose of reinforcing plate

2.3.2.2. Length of the flange plate

The effect of flange plate length on the response of reinforced connections was investigated in this research. To assess the effect of flange plate length on the behavior of connections, the responses of two specimens LF30-T and LF50-T are compared below.

The distributions of the RI for LF30-T and LF50-T on the beam bottom flange at the nose of the reinforcing plate are shown in Fig. 8. The maximum RI value of LF50-T is approximately 15% larger

than that of LF30-T. This indicates that a longer flange plate increases values of RI at the nose of the reinforcing plate. There is a possible explanation for this phenomenon:

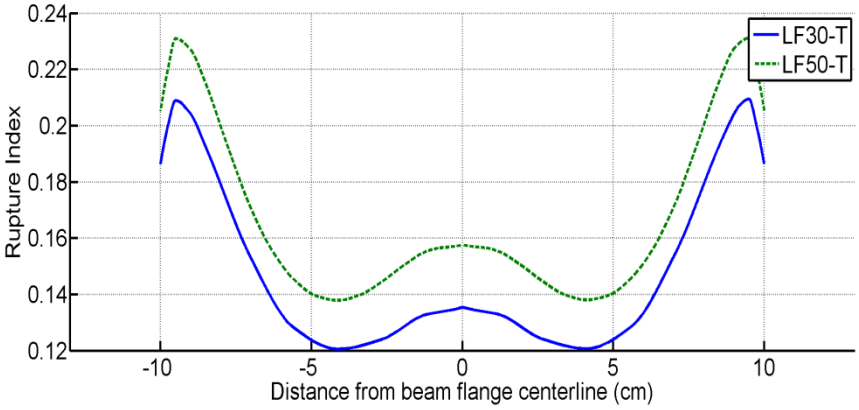

Figure 8. Distribution of rupture indices on beam flange at the nose of reinforcing plate

A longer flange plate results in a higher plastic strain at the nose of reinforcing plate due to an increase in the beam plastic rotation. Eqn. 1 shows that the higher plastic strain can results in higher RI value.

2.3.3. Global response of flange plate connections

In this section, the global behavior of models LF30 and LF30-T was evaluated before experimental studies. A displacement-control loading in the beam tip was induced in compliance with AISC seismic provisions loading history. Equivalent plastic strain contours for models LF30 and LF30-T are presented in Figure 9. The key observations from Fig. 9 are (1) the maximum plastic strain occurs at the end of the longitudinal fillet weld of model LF30 and (2) in models LF30 and LF30-T, plastic hinge forms away from the column flange into the beam beyond the nose of flange plates.
The moment at the column face versus story drift angle (θ) relationship for model LF30-T is shown in Fig. 10. Story drift angle is computed by dividing the total beam tip displacement by the distance from the beam tip to the column centerline. The hysteretic curve for model LF30 was identical to model LF30-T.

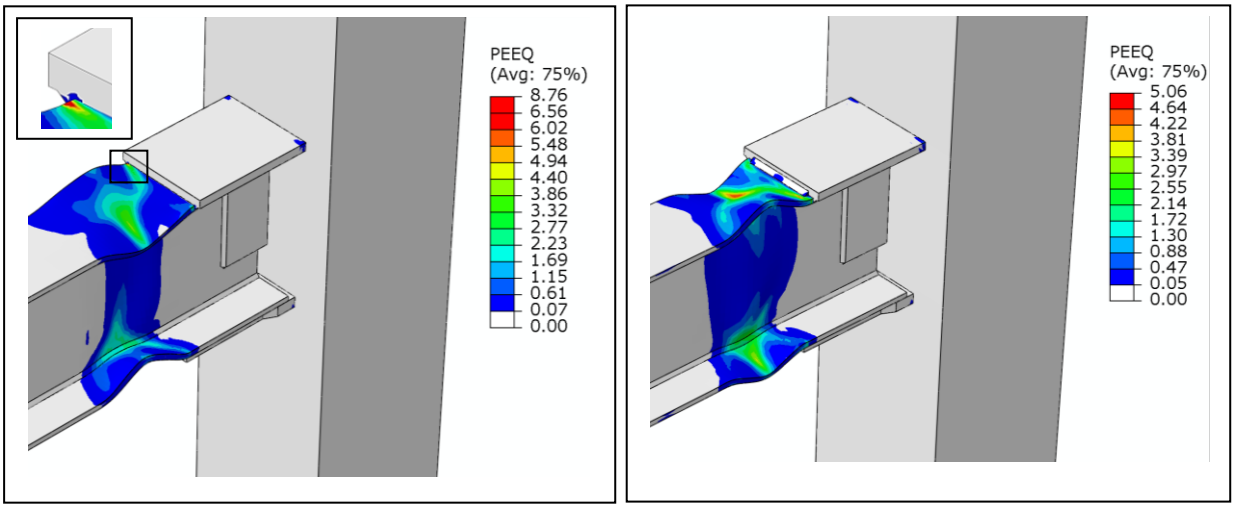

a) b)

Figure 9. Equivalent plastic strain contours for models a) LF30 and b) LF30-T

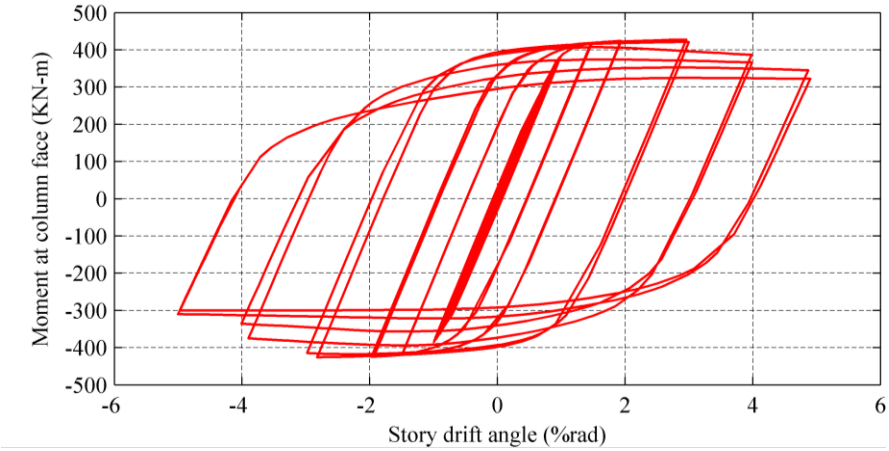

Figure 10. Cyclic response of model LF30-T

3. EXPRIMENTAL PROGRAM

Two full scale test specimens with the same dimensions and connection details of models LF30-T and LF30 were fabricated. The general configuration of the test setup is shown in Fig. 11. The column top and bottom were supported by real hinges. The beam was laterally braced in the vicinity of the plastic hinge and also near the beam end. The cyclic displacement proposed by AISC seismic provisions was applied at the tip of the beam by a hydraulic actuator.

The moment at the column face versus story drift angle (θ) relationship for the test specimen LF30-T is shown in Fig. 12. The cyclic response of test specimen LF30 was identical to LF30-T. The results showed fair agreement between both experimental (Fig. 12) and analytical (Fig. 10) responses. In order to have a good comparison between analytical and experimental results a combined plot is illustrated in Fig. 13. Both the test specimens achieved the AISC seismic provision requirements for special moment frames.

Figs. 14 and 15 show the test specimens LF30 and LF30-T at the end of the test. In the both test specimens, plastic hinge forms in the beam at the nose of flange plate. Such a result is desirable because the objective of the flange-plate connection is to force inelastic action in the beam away from the column face. In the specimen LF30, tearing was occurred at the groove weld joining the beam web to the beam flange at the plastic hinge region, as shown in Fig. 15. In contrast, no crack was observed in the specimen LF30-T. This indicates that a longer flange plate increases potential for fracture at the plastic hinge region.

Figure 11. Test setup configuration

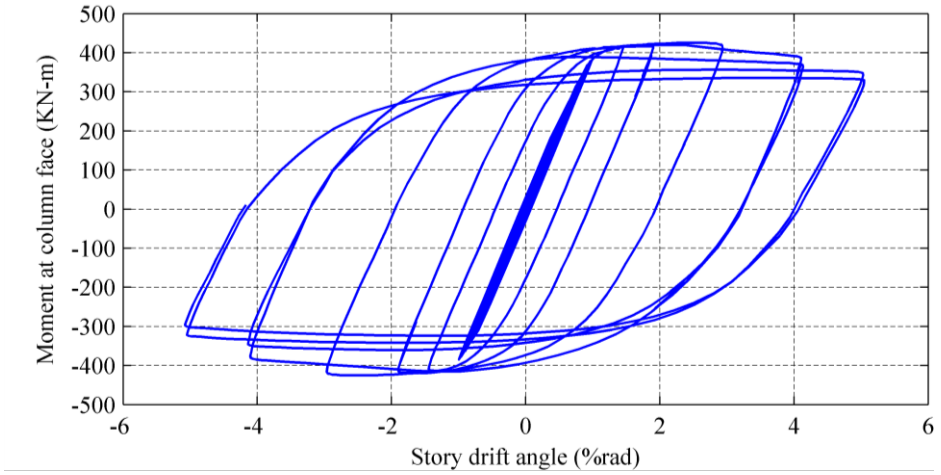

Figure 12. Moment at the column face versus story drift angel relationship

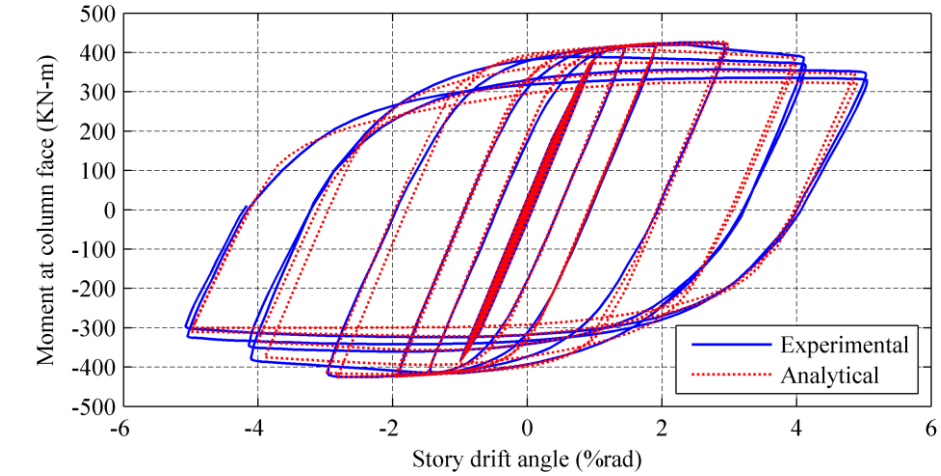

Figure 13. Comparison of the experimental and analytical results

Figure 14. Specimen LF30-T at the end of the test.

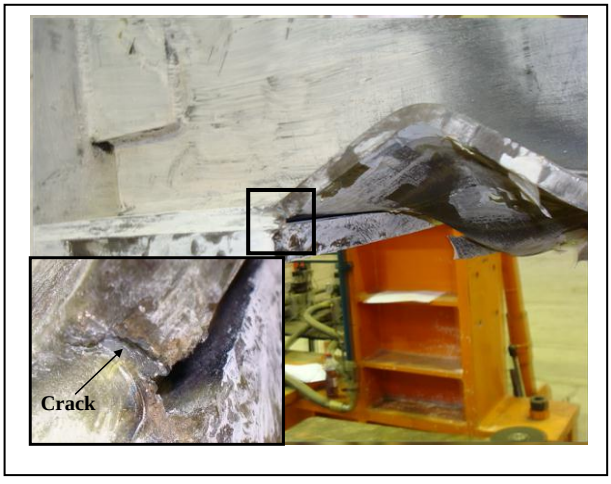

Figure 15. Specimen LF30 at the end of the test.

4. CONCLUSIONS

Two full-size specimens with flange plat connections were tested. Each specimen composed of a H-shaped steel beam with the dimensions of H-380×200×8×12 (mm) connected to a box column with the measurements of B-400 × 400 × 20 × 20 (mm). In the one of specimens, flange plates were joined to the beam flanges with longitudinal fillet welds only. The flange plates of other specimen were joined to the beam flanges with longitudinal and transverse fillet welds. Flange plate connections of test specimens achieved the AISC seismic provision requirements for special moment frames.

The key conclusions drawn from the analytical studies and the associated experimental results are:
1. In the test specimens, no damage was observed at the groove welds joining flange plates to column flange. Because use of flange plate reduces potential for fracture at column face.
2. Analytical analysis indicated that use of transverse fillet weld at the nose of flange plate will reduce potential for fracture at the end of longitudinal fillet welds. This result was confirmed by the tests conducted for two full-scale specimens. .
3. It is better that the required flange plate length be limited to shortest possible length using weld of higher strength and increasing weld thickness to the maximum allowable limit.

REFERENCES

Nakashima, M., Roeder, CW. and Maruoka, Y. (2000). Steel moment frames for earthquakes in United States and Japan. *J Struct Eng* **126:8**, 861–8.

Kim T., Whittaker AS., Gilani ASJ., Bertero VV. and Takhirov SM. (2002). Cover-plate and flange-plate steel moment-resisting connections. *Journal of Structural Engineering* **128:4**, 474–482.

Ricles JM., Fisher JW., Lu LW. and Kaufmann EJ. (2002). Development of improved welded moment connections for earthquake-resistant design. *Journal of Constructional Steel Research* **58:4**, 565–604.

Chen CC., Chen SW., Chung MD. and Lin MC. (2005). Cyclic behavior of unreinforced and rib-reinforced moment connections. *Journal of Constructional Steel Research* **61:6**, 1–21.

Tabar, A.M. and Deylami, A. (2004). Investigation of major parameters affecting instability of steel beams with RBS moment connections. *Steel and Composite Structures* **6:3**, 1475-1491.

Shiravand, M. and Deylami, A. (2010). Application of Full Depth Side Plate to Moment Connection of I-Beam to Double-I Column. *Advances in Structural Engineering* **13:6**, 1047-1062.

Adeli, M., Banazadeh, M. and Deylami, A. (2011). Bayesian approach for determination of drift hazard curves for generic steel moment-resisting frames in territory of Tehran. *International Journal of Civil Engineering* **9: 3**, 145-154.

Chen CC., Lin CC. and Tsai CL. (2004). Evaluation of reinforced connections between steel beams and box columns. *Engineering Structures* **13:5**, 1089–1092.

Kim T., Whittaker AS., Gilani ASJ., Bertero VV., Takhirov SM.and Ostertag C. (2004). Forensic studies of a large cover plat steel moment resisting connection. *The Structural Design of Tall Buildings*, 265–283.

Kaufmann, E. J. (1997). Dynamic tension tests of simulated moment resisting frame weld joints.Chicago. Steel Tips, Structural Steel Education Council. *American Institute of Steel Construction* .

Kim T., Whittaker AS., Gilani ASJ., Bertero VV. and Takhirov SM. (2002). Cover-plate and flange-plate steel moment-resisting connections. *Journal of Structural Engineering* **128:4**, 474–482.

Ricles JM., Fisher JW., Lu LW. and Kaufmann EJ. (2002). Development of improved welded moment connections for earthquake-resistant design. *Journal of Constructional Steel Research* **58:4**, 565–604.

Mao C., Ricles JM., Lu LW. and Fisher JW.(2001). Effect of local details on ductility of welded moment connections. *Journal of Structural Engineering* **127:9**, 1036–1044.

Hancock JW. and Mackenzie AC. (1976). On the mechanisms of ductile failure in high strength steels subjected to multi-axial stress states. *Journal of the Mechanics and Physics of Solids* **24:5**, 147–169.